



HAL
open science

Dielectric properties of Er-doped HfO₂ (Er 15%) grown by atomic layer deposition for high-kappa gate stacks

C. Wiemer, L. Lamagna, S. Baldovino, M. Perego, Sylvie Schamm-Chardon, Pierre-Eugène Coulon, O. Salicio, G. Congedo, S. Spiga, M. Fanciulli

► To cite this version:

C. Wiemer, L. Lamagna, S. Baldovino, M. Perego, Sylvie Schamm-Chardon, et al.. Dielectric properties of Er-doped HfO₂ (Er 15%) grown by atomic layer deposition for high-kappa gate stacks. Applied Physics Letters, 2010, 96 (18), pp.182901. 10.1063/1.3400213 . hal-01745025

HAL Id: hal-01745025

<https://hal.science/hal-01745025>

Submitted on 9 Apr 2018

HAL is a multi-disciplinary open access archive for the deposit and dissemination of scientific research documents, whether they are published or not. The documents may come from teaching and research institutions in France or abroad, or from public or private research centers.

L'archive ouverte pluridisciplinaire **HAL**, est destinée au dépôt et à la diffusion de documents scientifiques de niveau recherche, publiés ou non, émanant des établissements d'enseignement et de recherche français ou étrangers, des laboratoires publics ou privés.

Dielectric properties of Er – doped HfO₂ (Er ~ 15%) grown by atomic layer deposition for high- κ gate stacks

C. Wiemer, L. Lamagna, S. Baldovino, M. Perego, S. Schamm-Chardon, P. E. Coulon, O. Salicio, G. Congedo, S. Spiga, and M. Fanciulli

Citation: *Appl. Phys. Lett.* **96**, 182901 (2010); doi: 10.1063/1.3400213

View online: <https://doi.org/10.1063/1.3400213>

View Table of Contents: <http://aip.scitation.org/toc/apl/96/18>

Published by the [American Institute of Physics](#)

Articles you may be interested in

[Crystallinity of inorganic films grown by atomic layer deposition: Overview and general trends](#)

Journal of Applied Physics **113**, 021301 (2013); 10.1063/1.4757907

[Permittivity enhancement of hafnium dioxide high- \$\kappa\$ films by cerium doping](#)

Applied Physics Letters **93**, 182911 (2008); 10.1063/1.3023059

[High- \$\kappa\$ gate dielectrics: Current status and materials properties considerations](#)

Journal of Applied Physics **89**, 5243 (2001); 10.1063/1.1361065

[Incomplete elimination of precursor ligands during atomic layer deposition of zinc-oxide, tin-oxide, and zinc-tin-oxide](#)

The Journal of Chemical Physics **146**, 052802 (2017); 10.1063/1.4961459

[Atomic layer deposition of HfO₂ using HfCp\(NMe₂\)₃ and O₂ plasma](#)

Journal of Vacuum Science & Technology A: Vacuum, Surfaces, and Films **35**, 01B130 (2017); 10.1116/1.4972210

[Ion migration in crystalline and amorphous HfO_x](#)

The Journal of Chemical Physics **146**, 094508 (2017); 10.1063/1.4977453

Scilight

Sharp, quick summaries **illuminating**
the latest physics research

Sign up for **FREE!**

AIP
Publishing

Dielectric properties of Er-doped HfO₂ (Er~15%) grown by atomic layer deposition for high- κ gate stacks

C. Wiemer,^{1,a)} L. Lamagna,¹ S. Baldovino,² M. Perego,¹ S. Schamm-Chardon,³ P. E. Coulon,³ O. Salicio,¹ G. Congedo,¹ S. Spiga,¹ and M. Fanciulli^{1,2}

¹Laboratorio MDM, IMM-CNR, Via C. Olivetti 2, 20041 Agrate Brianza, Monza Brianza 20041, Italy

²Dipartimento di Scienza dei Materiali, Università degli Studi di Milano-Bicocca, Milano, Italy

³CEMES-CNRS and Université de Toulouse, nMat group, BP 94347, 31055 Toulouse Cedex 4, France

(Received 20 November 2009; accepted 30 March 2010; published online 5 May 2010)

Er-doped HfO₂ (Er~15%) films are grown by atomic layer deposition on Si(100). The characteristics of the doped oxide are compared with those of HfO₂. In Er-doped HfO₂, the stabilization of the cubic structure, together with the effect of the high polarizability of Er³⁺, allow to obtain a dielectric constant of ~33 after annealing at 900 °C. The insertion of Er within the metallic sublattice of HfO₂ reduces the net density of fixed charges, due to the creation of oxygen vacancies. For similar equivalent oxide thickness, lower leakage currents are measured for Er-doped HfO₂ than for HfO₂. © 2010 American Institute of Physics. [doi:10.1063/1.3400213]

In the search of alternative high-dielectric constant (high- κ) oxides, special attention has recently been devoted to doped HfO₂.^{1,2} Actually, small percentages of dopant elements have been demonstrated to stabilize the cubic fluorite (*c*) and tetragonal phases of HfO₂, thus enhancing its dielectric constant.^{3,4} In particular, doping HfO₂ with a rare earth element [i.e., Gd (Ref. 5)] has been calculated to stabilize the *c* phase for dopant percentages above 9.9%. The case of Er-doped HfO₂ (Er-HfO₂) is of particular interest since Er has one of the highest electronegativities and one of the lowest ionic radii of the lanthanide series, therefore resulting in a limited tendency to hydroxylation.⁶ The stabilization of the *c* phase in Er-HfO₂ has been demonstrated in films obtained with different deposition techniques. Incorporation of Er by reactive sputtering (Er~30%),⁷ and physical vapor deposition of Er-doped HfO₂ (Er~10–20%) lead to high κ values (~28–30) associated with low equivalent oxide thickness (EOT) and low leakage currents.^{8,9} Moreover, the insertion of a substitutional rare earth element in the oxide matrix can enhance the κ value due to the softening of the infrared-active transverse optical phonon modes.¹⁰ On the other hand, the introduction of a 3+ element, such as Er, in the metallic sublattice of HfO₂ may cause the formation of oxygen vacancies (OV), therefore reducing the performance of the metal-oxide-semiconductor (MOS) or memory device.⁹

In this letter, we report on the atomic layer deposition (ALD) of Er-HfO₂, with an Er content of 15%, aiming at the stabilization of the *c* phase. By combining different characterization techniques including time of flight (ToF)-secondary ion mass spectrometry (SIMS), x-ray diffraction (XRD), x-ray reflectivity (XRR), spectroscopic ellipsometry (SE), transmission electron microscopy (TEM), capacitance-voltage (C-V), and current density-voltage (J-V) measurements, we address the improved κ value and lower leakage current of Er-HfO₂ as compared with pure HfO₂. A high temperature postdeposition rapid thermal annealing (RTA) is found to promote a further increase of the κ value of Er-HfO₂.

Films were grown in a Savannah 200 (Cambridge Nanotech Inc.) ALD reactor at 300 °C on H-terminated n-type Si(100) using (iPrCp)₃Er and (MeCp)₂HfMe(OMe), respectively, as Er and Hf source, and O₃ (~200 g/Nm³) as oxygen source. HfO₂ was grown using the same recipe adopted for the ternary compound. The 15% Er content was achieved by tuning the ALD pulse ratio in an alternate Er₂O₃ and HfO₂ deposition. Smooth and uniform HfO₂ and Er-HfO₂ films were grown in the 3–30 nm thickness range varying the number of cycles between 25 and 300. RTA was performed at selected temperatures between 400 and 900 °C, in N₂ atmosphere, for one minute. The Er/Hf chemical ratio was checked by total reflection x-ray fluorescence and did not vary after RTA up to 900 °C. Stack thickness was measured by SE, XRR, and TEM.

As-grown Er-HfO₂ films within the 8–33 nm thickness range are crystallized, while thinner ones are amorphous. Crystallization of Er-HfO₂ occurs in the *c* structure¹¹ with a lattice parameter (*a*), equal to 5.06 ± 0.01 Å. Figure 1(a) shows the variation upon RTA at 900 °C of the diffraction patterns of Er-HfO₂ and HfO₂. HfO₂ is mostly crystallized in the monoclinic phase,¹¹ either before or after RTA. After RTA, Er-HfO₂ films thinner than 8 nm crystallize within the *c* phase, while this structure is maintained for films thicker than 8 nm. The grain size, measured from dark field TEM images, increases by 40% after RTA at 900 °C. In order to correctly simulate by Rietveld refinement the variation of the diffracted maxima, it is necessary to take into account both the increase in grain size and a decrease in the microstrain from 2.8 ± 0.1% to 2.0 ± 0.1%. RTA at 900 °C causes a densification of the high- κ layer as revealed by XRR analysis [Fig. 1(b)], corresponding to an increase in the electronic density of the order of 4% and a decrease in the layer thickness of ~5%. The interfacial layer (IL) thickness increases [Fig. 1(a)], from 1.3 ± 0.3 to 2.3 ± 0.3 nm. Electron energy loss spectroscopy (not shown) detected not only Si and O, but also Hf and Er species in the IL region. ToF SIMS profiles [Fig. 1(c)] confirm the increase of the IL thickness upon RTA and reveal a strong decrease in OH⁻ content concomitantly with a slight Si diffusion inside the oxide layer. The OH⁻ incorporation might be attributed to the formation of

^{a)}Author to whom correspondence should be addressed. Electronic mail: claudia.wiemer@mdm.imm.cnr.it.

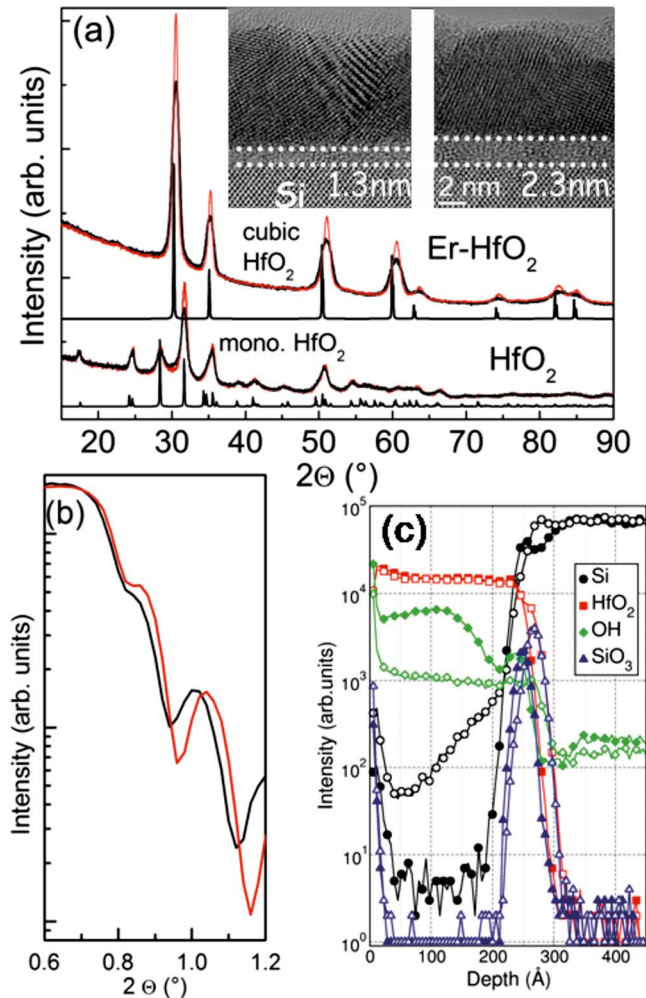


FIG. 1. (Color online) (a) XRD analysis of as-grown (black) and 900 °C annealed (red) 30 nm thick HfO₂ and Er-HfO₂. Inset: high resolution TEM of as-grown (left) and 900 °C annealed (right) 10 nm thick Er-HfO₂. (b) Detail of XRR analysis of as grown (black) and 900 °C annealed (red) 30 nm thick Er-HfO₂. (c) ToF SIMS profiles of as deposited (full symbols), and 900 °C annealed (open symbols) Er-HfO₂.

Er(OH)₃ species in as-grown films upon exposure to air.

C-V curves acquired at various frequencies on a 7.1 nm thick Er-HfO₂ film annealed at 900 °C are reported in Fig. 2(a), while in the inset the MOS behaviors of structures including Er-HfO₂ and HfO₂ films with similar EOT and annealed at 900 °C are compared. The C-V curves are rather well behaved with small frequency dispersion in accumulation. In the depletion region, the frequency dispersion and the stretch-out indicate a fairly high interface traps density, while the hysteresis loop is due to charge trapping phenomena in the oxide near the interface with Si(100). These features are probably connected to the strong oxidizing power of O₃ that, as reported,¹² may generate highly defective interfaces. Nevertheless, RTA reduces the trap density from 6×10^{12} to 1×10^{12} eV⁻¹ cm⁻² for the thinnest Er-HfO₂ layer, and from 2×10^{12} to 1×10^{12} eV⁻¹ cm⁻² for the thinnest HfO₂ film (evaluated with the Hill Coleman method¹³ at 10 kHz).

The flat band voltage (V_{FB}) is extracted from simulations of multifrequency C-V curves.¹⁴ In order to separate the contribution to the V_{FB} shift of the oxide charges from the one of the effective metal work function, V_{FB} versus EOT curves were analyzed [Fig. 2(b)]. By comparing the

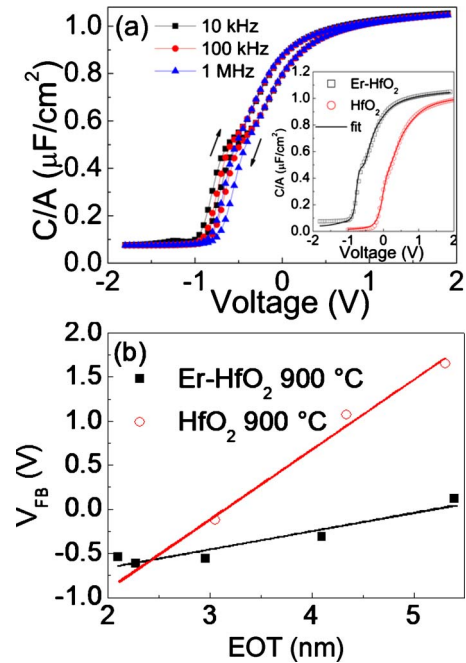


FIG. 2. (Color online) (a) C-V curves corrected for series resistance for an annealed Er-HfO₂ film with double sweep. Inset: C-V curves, acquired at 100 kHz, including 7.1 nm thick Er-HfO₂ film (squares) and 4.0 nm thick HfO₂ film (circles) after RTA 900 °C, with Al gates. (b) V_{FB} vs EOT plots of Er-HfO₂ (squares) and HfO₂ (circles) films annealed at 900 °C.

slopes obtained from MOS structures including, after RTA at 900 °C, Er-HfO₂ and HfO₂, we estimate that the net amount of negative fixed charges is reduced (from low 10^{13} cm⁻² for HfO₂ to mid 10^{12} cm⁻² for Er-HfO₂). This variation associated to the doping of HfO₂ with a rare earth element has been reported^{7,15} and interpreted as an increase in positive fixed charges. A possible source of positive fixed charges, directly connected to the insertion of a 3+ element, is the creation of OV.⁵ Therefore, the reduction in the negative fixed charges is due to electrical compensation with positive charges induced by the Er doping via OV. Moreover, the dependence of V_{FB} on EOT reveals that the fixed oxide charge is mainly distributed either at the Si(100)/IL or at the IL/high- κ interface.¹⁶ This hypothesis is consistent with the tendency of the OV to segregate at the Si/HfO₂ interface.¹⁷

The EOT is extracted by fitting the C-V curves at 100 kHz including quantum mechanical corrections (Fig. 2).¹⁴ For the as-grown layers, a κ value of 18 ± 1 for HfO₂ and 27 ± 1 for Er-HfO₂ are extracted (Fig. 3). After RTA, the κ value of HfO₂ is slightly reduced to 16 ± 1 , being still in the range of the values expected for monoclinic HfO₂. For Er-HfO₂, after RTA the κ value increases to 33 ± 1 , resulting even higher than the one calculated for *c* HfO₂ (29, 18). This unexpected behavior will be further discussed.

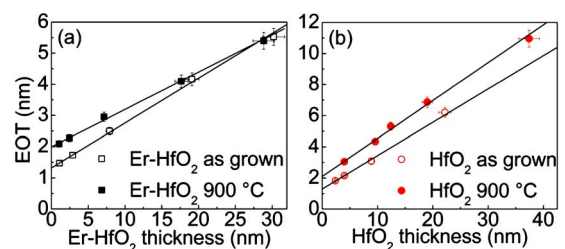


FIG. 3. (Color online) EOT vs physical thickness. (a) Er-HfO₂; (b) HfO₂, as-grown (open symbols), 900 °C annealed (full symbols).

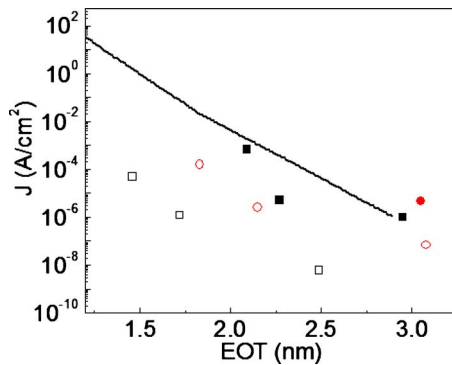


FIG. 4. (Color online) J versus EOT for HfO_2 (circles) and Er-HfO_2 (squares). Open symbols: as-grown, full symbols: annealed at 900°C . The curve for SiO_2 (Ref. 22) is also displayed.

The dependence of the EOT on the thickness for as-grown Er-HfO_2 samples is linear; therefore all the κ values are the same regardless of the amorphous or crystallized structure of the films. Probably, Er doping contributes to the increase in the κ value expected for amorphous HfO_2 (22, Ref. 19) due to its polarizability. Although peculiar aspects related to the low dimension of these thin films cannot be ruled out, their short range order could be very similar to the one observed in crystallized samples, hence giving a very similar κ value. This hypothesis is supported by the crystallization after RTA of thin amorphous Er-HfO_2 layers in the c phase instead than in the monoclinic one.

In Fig. 3 the fit intercepts reveals the presence of an IL. The EOT of the IL is 1.3 nm for as deposited films and 2.0 nm after RTA, regardless of the Er content. Therefore, the EOT of the IL seems not to be affected by Er doping, differently from what might be expected due to the creation of OV when doping with a 3+ element.⁹ Considering the EOT and the physical thickness of the IL, we deduce that its κ is close to the one of SiO_2 .

Figure 4 shows the gate leakage current densities of Er-HfO_2 and HfO_2 , at $|V_g - V_{\text{FB}}| = 1$ V. In literature both weak increases in the leakage current upon doping with a rare earth element^{7,20} and strong reductions^{8,15} are reported. In our case, for similar EOT values, doping with Er decreases the leakage current, due to the increased physical thickness. However, this decrease is not so strong, probably because the OV can serve as traps for Poole-Frenkel conduction mechanism. The increased leakage values after RTA further confirm that conduction mechanisms might be influenced by different chemical compositions and crystallographic structures.

It seems reasonable to assume that the introduction of OV modifies the metal-O and O-O bondings therefore affecting κ . Actually, the κ value measured for as-grown Er-HfO_2 is slightly lower than the one calculated for c HfO_2 , while it increases upon RTA. The measured value of a does not vary with RTA. Therefore, no variation in the lattice volume can be correlated with the κ increase. On the other hand, the increase in grain size with annealing could contribute to the κ enhancement because of the corresponding increase in the crystallized fraction within the film. The high κ value of c Er-HfO_2 , might also be explained referring to the higher polarizability of Er^{3+} ions than Hf^{4+} .²¹ For the measured a value, the corresponding cation-O bond lengths are 2.19 Å. In the as deposited layers, the presence of OH^-

groups, which are preferentially bonded to Er due to its hygroscopic nature, together with the presence of 2+ charged OV, cause a distortion of the O sublattice within the c structure, since typical bond lengths of Er-OH are of the order of 2.3–2.4 Å.¹¹ After RTA, as the a does not vary, the release of OH^- is accompanied by the relaxation of the microstrain, mostly related to the rearrangement of the O sublattice that might increase the κ value. It is worth noticing that for RTA at 400, 600 and 750 °C no modifications of both the crystallographic structure and the OH^- content are found and that, correspondingly, the κ value does not change (not shown).

In summary, we have demonstrated the improved dielectric properties of Er-HfO_2 films grown by ALD as compared with parental HfO_2 . A κ value of ~ 33 was obtained after RTA at 900°C , due to the increase in the crystallized fraction, the reduction of microstrain and of the OH^- content. At comparable EOT, lower leakage currents than those obtained for HfO_2 are measured for Er-HfO_2 without any increase in the EOT of the IL being induced by the Er doping.

This work was supported by the European FP6-Program “REALISE” (Grant No. IST-NMP 016172).

- ¹J. Niinistö, K. Kukli, M. Heikkilä, M. Ritala, and M. Leskela, *Adv. Eng. Mater.* **11**, 223 (2009).
- ²P. R. Chalker, M. Werner, S. Romani, R. J. Potter, K. Black, H. C. Aspinnall, A. C. Jones, C. Z. Zhao, S. Taylor, and P. N. Heys, *Appl. Phys. Lett.* **93**, 182911 (2008).
- ³D. Fischer and A. Kersch, *Appl. Phys. Lett.* **92**, 012908 (2008).
- ⁴W. He, L. Zhang, D. S. H. Chan, and B. J. Cho, *IEEE Electron Device Lett.* **30**, 623 (2009).
- ⁵C. K. Lee, E. Cho, H. S. Lee, C. S. Hwang, and S. Han, *Phys. Rev. B* **78**, 012102 (2008).
- ⁶G. Scarel, A. Svane, and M. Fanciulli, in *Rare Earth Oxide Thin Films: Growth, Characterization, and Applications*, Topics in Applied Physics, edited by M. Fanciulli and G. Scarel (Springer, Berlin 2006), Vol. 106, p. 1.
- ⁷J. Chen, X. P. Wang, M.-F. Li, S. J. Lee, M. B. Yu, C. Shen, and Y. C. Yeo, *IEEE Electron Device Lett.* **28**, 862 (2007).
- ⁸S. Govindarajan, T. S. Bösccke, P. Sivasubramani, P. D. Kirsch, B. H. Lee, H. H. Tseng, R. Jammy, U. Schröder, S. Ramanathan, and B. E. Gnade, *Appl. Phys. Lett.* **91**, 062906 (2007).
- ⁹S. Ramanathan, A. Karthikeyan, S. A. Govindarajan, and P. D. Kirsch, *J. Vac. Sci. Technol. B* **26**, L33 (2008).
- ¹⁰G. Dutta, *Appl. Phys. Lett.* **94**, 012907 (2009).
- ¹¹Inorganic crystal structure database, file 53033 for cubic HfO_2 and 27313 for monoclinic HfO_2 , file 34475 for $\text{ErO}(\text{OH})$ and file 200097 for $\text{Er}(\text{OH})_3$, Fachinformationzentrum Karlsruhe (2009).
- ¹²S. Baldovino, S. Spiga, G. Scarel, and M. Fanciulli, *Appl. Phys. Lett.* **91**, 172905 (2007).
- ¹³W. A. Hill and C. C. Coleman, *Solid-State Electron.* **23**, 987 (1980).
- ¹⁴G. Apostolopoulos, G. Vellianitis, A. Dimoulas, J. C. Hooker, and T. Conard, *Appl. Phys. Lett.* **84**, 260 (2004); Metal-insulator-semiconductor CV fitting (MISFIT) software.
- ¹⁵C. Adelman, V. Sriramkumar, S. Van Elshocht, P. Lehnen, T. Conard, and S. De Gendt, *Appl. Phys. Lett.* **91**, 162902 (2007).
- ¹⁶V. S. Kaushik, B. J. O’Sullivan, G. Pourtois, N. Van Hoornick, A. Delabie, S. Van Elshocht, W. Deweerdt, T. Schram, L. Pantisano, E. Rohr, L. Ragnarsson, S. De Gendt, and M. Heyns, *IEEE Trans. Electron Devices* **53**, 2627 (2006).
- ¹⁷C. Tang, B. Tuttle, and R. Ramprasad, *Phys. Rev. B* **76**, 073306 (2007).
- ¹⁸X. Zhao and D. Vanderbilt, *Phys. Rev. B* **65**, 233106 (2002).
- ¹⁹D. Ceresoli and D. Vanderbilt, *Phys. Rev. B* **74**, 125108 (2006).
- ²⁰X. P. Wang, M.-F. Li, C. Ren, X. F. Yu, C. Shen, H. H. Ma, A. Chin, C. X. Zhu, J. Ning, M. B. Yu, and D.-L. Kwong, *IEEE Electron Device Lett.* **27**, 31 (2006).
- ²¹R. D. Shannon and R. X. Fischer, *Phys. Rev. B* **73**, 235111 (2006).
- ²²J. M. J. Lopes, E. Durgun Ozben, M. Roeckerath, U. Littmark, R. Luptak, St. Lenk, M. Luysberg, A. Besmehn, U. Breuer, J. Schubert, and S. Mantl, *Microelectron. Eng.* **86**, 1646 (2009).